On-Chip Millionfold Sample Stacking Using Transient Isotachophoresis

Byoungsok Jung,[†] Rajiv Bharadwaj,[‡,§] and Juan G. Santiago*,[†]

Department of Mechanical Engineering, and Department of Chemical Engineering, Stanford University, Stanford, California 94305

We present a simple and robust isotachophoresis (ITP) method that can be integrated with microchip-based capillary electrophoresis (CE) devices to achieve million-fold sample stacking. We performed an experimental parametric study to show the effects of initial sample ion concentration, leading ion concentration, and trailing ion concentration on ITP stacking. We also discuss the usefulness and limitations of a simple one-dimensional nondispersive model and a scaling analysis for dispersion rate. We found that a single-column ITP configuration together with electroosmotic flow suppression and high leading ion concentration provide high-performance ITP and can be integrated readily with CE separation. We demonstrated detection of trace of 100 fM Alexa Fluor 488 (signal-to-noise ratio of 11) with a concentration increase of a factor of 2×10^6. Application of our ITP/CE protocol to the stacking and separation of negatively charged fluorescent tracers (Alexa Fluor 488 and bodipy) resulted in a concentration increase of 6.4×10^4 and a signal increase of 4.5×10^5. The ITP/CE protocol can be performed with a standard microchannel cross design or simple flow control. The method can be implemented with available off-the-shelf chip systems using off-the-shelf voltage control systems and buffer chemistries.

On-chip capillary electrophoresis (CE) has been the subject of extensive research over the past decade.[1,2] Microfabrication provides advantages over traditional capillary systems including rapid separation, reduced sample volumes, and integration with other microfluidic functions. However, the limit of detection (LOD) of on-chip CE systems can be limited by associated small sample volumes and the shallow depth of etched channels (typically 10−20 μm), which limits path length available to photodetectors. One way of improving sensitivity is to integrate an online sample stacking method. Stacking enables the use of less sensitive detection modality, such as UV absorption.[3] On-chip injections

with isotachophoresis is also more robust to errors in voltage activation times and field ratios used in an electrokinetic injection than a simple uniform electrolyte CE type injection since precon-centration reduces effective sample plug immediately prior to the CE mode. On-chip stacking methods include electromigration-based processes such as field-amplified sample stacking,[4,5] large-volume sample stacking (FASS),[6] and isotachophoresis (ITP);[7,8] affinity-based sample stacking methods including sweeping[9] and solid-phase extraction;[10] and electrophoretic focusing methods such as isoelectric focusing[11] and temperature gradient focusing.[12]

Electromigration-based sample stacking leverages spatial gradients of electrophoretic velocity of sample analytes as effected by gradients in ion density, mobility, or solvent viscosity. Table 1 highlights a representative summary of highest signal enhancement of electromigration-based preconcentration methods. Included are on-chip ITP,[13−17] on-chip FASS,[4,5,18−21] on-chip large-volume sample stacking (LVSS),[22] capillary ITP,[23−28] capillary FASS,[29−31] capillary LVSS,[32−38] and capillary field-amplified sample

(4) Jacobson, S. C.; Ramsey, J. M. *Electrophoresis* **1995,** *16,* 481−486.
(5) Lichtenberg, J.; Verpoorte, E.; de Rooij, N. F. *Electrophoresis* **2001,** *22,* 258−271.
(6) Li, J. J.; Wang, C.; Kelly, J. F.; Harrison, D. J.; Thibault, P. *Electrophoresis* **2000,** *21,* 198−210.
(7) Walker, P. A.; Morris, M. D.; Burns, M. A.; Johnson, B. N. *Anal. Chem.* **1998,** *70,* 3766−3769.
(8) Kaniansky, D.; Masar, M.; Bielcikova, J.; Ivanyi, F.; Eisenbeiss, F.; Stanislawski, B.; Grass, B.; Neyer, A.; Johnck, M. *Anal. Chem.* **2000,** *72,* 3596−3604.
(9) Palmer, J.; Burgi, D. S.; Munro, N. J.; Landers, J. P. *Anal. Chem.* **2001,** *73,* 725−731.
(10) Kutter, J. P.; Jacobson, S. C.; Ramsey, J. M. *J. Microcolumn Sep.* **2000,** *12,* 93−97.
(11) Herr, A. E.; Molho, J. I.; Drouvalakis, K. A.; Mikkelsen, J. C.; Utz, P. J.; Santiago, J. G.; Kenny, T. W. *Anal. Chem.* **2003,** *75,* 1180−1187.
(12) Ross, D.; Locascio, L. E. *Anal. Chem.* **2002,** *74,* 2556−2564.
(13) Wainright, A.; Williams, S. J.; Ciambrone, G.; Xue, Q. F.; Wei, J.; Harris, D. *J. Chromatogr., A* **2002,** *979,* 69−80.
(14) Vreeland, W. N.; Williams, S. J.; Barron, A. E.; Sassi, A. P. *Anal. Chem.* **2003,** *75,* 3059−3065.
(15) Zhang, B.; Liu, H.; Karger, B. L.; Foret, F. *Anal. Chem.* **1999,** *71,* 3258−3264.
(16) Jeong, Y. W.; Choi, K. W.; Kang, M. K.; Chun, K. J.; Chung, D. S. *Sens. Actuators, B* **2005,** *104,* 269−275.
(17) Xu, Y. C.; Vaidya, B.; Patel, A. B.; Ford, S. M.; McCarley, R. L.; Soper, S. A. *Anal. Chem.* **2003,** *75,* 2975−2984.
(18) Kutter, J. P.; Ramsey, R. S.; Jacobson, S. C.; Ramsey, J. M. *J. Microcolumn Sep.* **1998,** *10,* 313−319.
(19) Yang, H.; Chien, R. L. *J. Chromatogr., A* **2001,** *924,* 155−163.
(20) Beard, N. R.; Zhang, C. X.; deMello, A. J. *Electrophoresis* **2003,** *24,* 732−739.
(21) Bharadwaj, R.; Santiago, J. G. *J. Fluid Mech.* **2005,** *543,* 57−92.
(22) Li, J. J.; LeRiche, T.; Tremblay, T. L.; Wang, C.; Bonneil, E.; Harrison, D. J.; Thibault, P. *Mol. Cell. Proteomics* **2002,** *1,* 157−168.
(23) Bondoux, G.; Jandik, P.; Jones, W. R. *J. Chromatogr.* **1992,** *602,* 79−88.

* To whom correspondence should be addressed. E-mail: juan.santiago@stanford.edu. Fax: (650) 723-7657.
† Department of Mechanical Engineering.
‡ Department of Chemical Engineering.
§ Current address: Caliper Life Sciences, 605 Fairchild Dr., Mountain View, CA 94043.
(1) Bruin, G. J. M. *Electrophoresis* **2000,** *21,* 3931−3951.
(2) Auroux, P. A.; Iossifidis, D.; Reyes, D. R.; Manz, A. *Anal. Chem.* **2002,** *74,* 2637−2652.
(3) Landers, J. P. *Handbook of Capillary Electrophoresis,* 2nd ed.; CRC Press: Boca Raton, FL, 1997.

Table 1. Selected Electromigration-Based Sample Stacking Methods[a]

method and ref	detection/ device	sample	electrolyte	SI	comments
FASS[19]	fl/chip	fluorescein sodium salt	0.1 mM HEPES and 0.2 mM NaCl 100 mM HEPES and 200 mM NaCl	100	five-channel geometry RT ≈ 1 min.
ITP[13]	fl/chip	eTags	LE: 25 mM imidazole, 20 mM HCl TE: 160 mM imidazole, 40 mM HEPES	530	highest on-chip ITP stacking prior to current work RT = 1−2 min
FASS[29]	UV/cap.	Dese, amino	45 mM NaH_2PO_4 and 15 mM Na_2HPO_4, 60% v/v 1-propanol	1000	RT = 4−6 min, L = 24.6 cm
LVSS[33]	UV/cap.	maleic, fumaric acids, bromide, nitrate	1 mM phosphoric acid, 40 mM potassium dihydrogen phosphate	300	RT = 5−10 min, L = 61 cm
FASI[38]	UV/cap.	bromide, nitrate, bromate	75 mM phosphate, DI water	1000	RT = 15−17 min, L = 25 cm
ITP[25]	UV/cap.	NXX-066	LE: 10 mM NaOH titrated with H_3PO_4, TE: 6.13 mM tetrahexylammonium chloride	5500	highest ITP stacking prior to current work RT = 6−10 min L = 53.5 cm
ITP (current work)	fl/chip	Alexa Fluor 488	LE: 1 M NaCl, TE: 5 mM HEPES	(2E6)	RT = 2 min

[a] Columns indicate method used (and reference number), detection mode (fl and UV for fluorescence and ultraviolet detection, respectively), type of device used (chip for microchip and cap. for capillary), sample analyte, electrolyte chemistry(ies), signal increase, and various comments (RT and L indicate run time and separation channel length, respectively).

injection (FASI).[38−41] For FASS, the highest signal enhancement factor has been typically limited to 1000-fold using capillaries[29,38] and 100-fold using microchips.[19,20] We demonstrated a 1000-fold signal enhancement using a hybrid stacking method that combined aspects of FASS with the mobility-based segregation dynamics of ITP.[42] The highest reported ITP signal enhancement factor has been roughly 500-fold for microchip experiments[13,16] and 5500-fold for capillaries.[25] The latter is, to our knowledge, the highest demonstrated signal increase for a single-step, electromigration-based preconcentration method prior to the current work. Millionfold signal increase was achieved by Quirino and Terabe,[39] but by combining two sample stacking methods (FASI and sweeping) in series in a 10-min assay involving at least two manual buffer exchange steps. Very recently, Wang et al. reported millionfold stacking of GFP using so-called electrokinetic trapping caused by what they suggested is an extended space charge layer at the interface between micro- and nanometer-scale channels in a custom-built chip.[43]

ITP uses multiple electrolytes where electrophoretic mobilities of sample ions are less than that of a leading electrolyte (LE) and greater than that of a trailing electrolyte (TE).[44] Individual species of the sample form narrow zones between the LE and TE and migrate with the same velocity ("isotacho" means equal velocity). With judicious choice of LE and TE chemistry, ITP is fairly generally applicable, can be accomplished with samples initially dissolved in either or both the TE and LE electrolytes, and (unlike FASS) does not require very low electrical conductivity background electrolytes. One disadvantage is that it requires some a priori knowledge of electrophoretic mobilities of sample ions. Kendall and Crittenden[45] first demonstrated ITP using rare earth metals and simple acids.[46] ITP is often combined with CE as a preseparation sample stacking method. Foret et al.[47] first demonstrated coupled-column ITP for traditional capillary devices, and single-column ITP was first developed by Jandik and Jones.[48] ITP was first implemented on chip by Walker and Morris,[7] and combination with on-chip CE has been demonstrated by many researchers.[15,49−52]

(24) Thompson, T. J.; Foret, F.; Vouros, P.; Karger, B. L. *Anal. Chem.* **1993**, *65*, 900−906.
(25) Enlund, A. M.; Schmidt, S.; Westerlund, D. *Electrophoresis* **1998**, *19*, 707−711.
(26) Riaz, A.; Kim, B.; Chung, D. S. *Electrophoresis* **2003**, *24*, 2788−2795.
(27) Wang, C. C.; McCann, W. P.; Beale, S. C. *J. Chromatogr., B* **1996**, *676*, 19−28.
(28) Kong, Y.; Zheng, N.; Zhang, Z. C.; Gao, R. Y. *J. Chromatogr., B* **2003**, *795*, 9−15.
(29) Zhang, C. X.; Thormann, W. *Anal. Chem.* **1996**, *18*, 2523−2532.
(30) Soga, T.; Inoue, Y.; Ross, G. A. *J. Chromatogr., A* **1995**, *718*, 421−428.
(31) Zhao, Y. P.; Lunte, C. E. *Anal. Chem.* **1999**, *71*, 3985−3991.
(32) Burgi, D. S. *Anal. Chem.* **1993**, *65*, 3726−3729.
(33) He, Y.; Lee, H. K. *Anal. Chem.* **1999**, *71*, 995−1001.
(34) Boden, J.; Darius, M.; Bachmann, K. *J. Chromatogr., A* **1995**, *716*, 311−317.
(35) Albert, M.; Debusschere, L.; Demesmay, C.; Rocca, J. L. *J. Chromatogr., A* **1997**, *757*, 291−296.
(36) Timerbaev, A. R.; Fukushi, K.; Miyado, T.; Ishio, N.; Saito, K.; Motomizu, S. *J. Chromatogr., A* **2000**, *888*, 309−319.
(37) Baryla, N. E.; Lucy, C. A. *Electrophoresis* **2001**, *22*, 52−58.
(38) Quirino, J. P.; Terabe, S. *J. Chromatogr., A* **1999**, *850*, 339−344.
(39) Quirino, J. P.; Terabe, S. *Anal. Chem.* **2000**, *72*, 1023−1030.
(40) Chen, Z. L.; Lin, J. M.; Naidu, R. *Anal. Bioanal. Chem.* **2003**, *375*, 679−684.
(41) Guan, F. Y.; Wu, H. F.; Luo, Y. *J. Chromatogr., A* **1996**, *719*, 427−433.
(42) Jung, B.; Bharadwaj, R.; Santiago, J. G. *Electrophoresis* **2003**, *24*, 3476−3483.

(43) Wang, Y. C.; Stevens, A. L.; Han, J. Y. *Anal. Chem.* **2005**, *77*, 4293−4299.
(44) Bocek, P.; Deml, M.; Gebauer, P.; Dolnik, V. *Analytical Isotachophoresis*; VCH: New York, 1988.
(45) Kendall, J.; Crittenden, E. D. *Proc. Natl. Acad. Sci. U.S.A.* **1923**, *9*, 75.
(46) Vesterberg, O. *J. Chromatogr.* **1989**, *480*, 3−19.
(47) Foret, F.; Sustacek, V.; Bocek, P. *J. Microcolumn Sep.* **1990**, *2*, 229−233.
(48) Jandik, P.; Jones, W. R. *J. Chromatogr.* **1991**, *546*, 431−443.
(49) Bodor, R.; Madajova, V.; Kaniansky, D.; Masar, M.; Johnck, M.; Stanislawski, B. *J. Chromatogr., A* **2001**, *916*, 155−165.
(50) Kurnik, R. T.; Boone, T. D.; Nguyen, U.; Ricco, A. J.; Williams, S. J. *Lab Chip* **2003**, *3*, 86−92.
(51) Wainright, A.; Nguyen, U. T.; Bjornson, T.; Boone, T. D. *Electrophoresis* **2003**, *24*, 3784−3792.
(52) Xu, Z. Q.; Ando, T.; Nishine, T.; Arai, A.; Hirokawa, T. *Electrophoresis* **2003**, *24*, 3821−3827.

In this paper, we describe a simple and robust method to integrate ITP with CE on a standard microfluidic chip. We demonstrate millionfold concentration increase in a fast, single-step electromigration assay. We present an experimental parametric study of ITP to explore the effects of concentrations of LE, TE, and sample analytes on stacked sample concentration and peak width. We also compare these results with the trends predicted by a simple nondispersive, closed-form, analytical model for ITP electromigration. Together, the results demonstrate a process by which to optimize ITP performance and predict trends. The results also provide validation data for more comprehensive models. Our ITP/CE injection, stacking, and separation method requires only a simple channel configuration, is performed with simple voltage control, and can be applied to off-the-shelf microchips.

THEORY

In the next two sections, we present a simple electromigration model and scaling arguments for dispersion rate to deduce strategies for optimizing ITP processes. More comprehensive models of ITP that include electromigration and diffusion of multiple species (although not the effects of convective dispersion) are given by Schwer et al.[53] and Martens et al.[54]

Nondispersive 1D Electromigration Model. The general transport of ions is governed by a conservation law for dilute species

$$\frac{\partial C_i}{\partial t} + \alpha \vec{u} \cdot \nabla C_i = - \nu_i \vec{\nabla} \cdot (C_i \vec{E}) + \frac{1}{Pe} D_i \nabla^2 C_i \qquad (1)$$

where C_i is the molar concentration of ion i, ν_i is the electrophoretic mobility, E is the electric field, and D_i is the diffusion coefficient. The parameters are defined as $Pe = E_0 \nu_0 \delta / D_0$ and $\alpha = - \epsilon \zeta_0 / (\mu \nu_0)$, where μ, ζ_0, and δ are respectively the viscosity, the characteristic scales for zeta potential, and the length of stacked sample zone. Pe is the electric Peclet number, a measure of the ratio of diffusion time to electromigration time. α is the ratio of electroosmotic mobility to electrophoretic mobility. To achieve high sample stacking, both diffusion and advective dispersion should be minimized (large Pe and small α). This is the case of high E with suppressed electroosmotic mobility. A detailed description will be shown in the next section.

We consider a model ITP system consisting of a leading ion, LE^-, sample ion, S^-, a trailing ion, TE^-, and common counterion, A^+. The following expression shows concentration adjustment between the two zones in this simplified ITP process[44,55]

$$C_{S,final} = C_{LE} \frac{\nu_S (\nu_A + |\nu_{LE}|)}{\nu_{LE} (\nu_A + |\nu_S|)} \qquad (2)$$

Here, the adjusted sample concentration, $C_{S,final}$, is only a function

of the LE concentration and electrophoretic mobilities (and not a function of, for example, TE concentration).

The degree of stacking in this simple ITP process can be characterized in terms of either concentration increase, CI or signal increase, SI. CI refers to stacked sample concentration divided by the original sample concentration. We use SI to refer to the ratio of the signal detected with sample preconcentration (e.g., at some downstream location after an electrophoretic separation) to the signal obtained without stacking.[42] For the current model, $CI = C_{S,final}/C_{S,initial}$, where $C_{S,final}$ is given by eq 2. This suggests that CI increases in direct proportion with LE concentration and CI is (conveniently) inversely proportional to initial sample concentration. We shall see that both of these predicted trends are correct for realistic ITP conditions and so this analysis is useful in optimizing practical ITP processes. However, we shall also see that other observed trends, such as the dependence of stacked sample concentration on initial sample concentration (for fixed applied potential), are not captured by this simple model.

Practical Concerns in the Implementation of ITP: Scaling Analysis of Dispersion Rate. In this section, we present some scaling arguments, which, together with the simple model above, suggest strategies to optimize ITP in practice. The model presented above neglects the effects of molecular diffusion and convective dispersion on stacked sample concentration. (We here use the term dispersion to refer to both molecular diffusion and convective dispersion.) ITP has gradients of ion density and species mobility, which leads to axial gradients in the electric field and gradients of electrophoretic velocities of ionic species and electroosmotic velocity of bulk liquid.[21] Electroosmotic velocity gradients are particularly important in determining dispersion. For any two regions of the channel, the electroosmotic velocity mismatch can be expressed as

$$\frac{U_{eof,1}}{U_{eof,2}} = \frac{\zeta_1 E_1}{\zeta_2 E_2} \cong \gamma^{-1+b} \qquad (3)$$

where $U_{eof,1}$ and $U_{eof,2}$ are the electroosmotic velocities of the two regions (e.g., in practical ITP, the regions containing LE and TE). In each channel region, U_{eof} is determined by the applied electric field, local conductivity, and local value of electroosmotic mobility. The rightmost term in eq 3 is one model for this velocity ratio, where γ is the electrical conductivity ratio of the two zones and b represents zeta potential (ζ) dependence on the concentration of electrolyte ($\zeta \sim C^b$) (the -1 term in the exponent captures the inverse dependence of conductivity on ion density). The value of b depends on the chemistry of the channel surface and the electrolyte solution; a typical range is between -0.2[56] and -0.3.[57] This mismatch in EOF velocity generates a pressure gradient that causes sample dispersion and lowers stacking efficiency.[21] These simple arguments suggest that EOF suppression is critical to optimizing the stacking efficiency of ITP.

In the limit of negligible EOF velocities (i.e., perfectly suppressed EOF), the dominant source of dispersion in ITP will be

(53) Schwer, C.; Gas, B.; Lottspeich, F.; Kenndler, E. *Anal. Chem.* **1993**, *65*, 2108−2115.
(54) Martens, J. H. P. A.; Reijenga, J. C.; Boonkkamp, J. H. M. T.; Mattheij, R. M. M.; Everaerts, F. M. *J. Chromatogr., A* **1997**, *772*, 49−62.
(55) Everaerts, F. M.; Beckers, J. L.; Verheggen, T. P. E. M., V. *Isotachophoresis. Theory, Instrumentation and Applications*; Elsevier: Amsterdam, 1976.
(56) Scales, P. J.; Grieser, F.; Healy, T. W.; White, L. R.; Chan, D. Y. C. *Langmuir* **1992**, *8*, 965−974.
(57) Yao, S. H.; Hertzog, D. E.; Zeng, S. L.; Mikkelsen, J. C.; Santiago, J. G. *J. Colloid Interface Sci.* **2003**, *268*, 143−153.

molecular diffusion. We can define a sample ion Peclet number in terms of the electrophoretic velocity of the sample and the width of the stacked sample zone,[58]

$$Pe_s = \frac{E_\delta v_s}{D}\left(\frac{l}{\mathrm{CI}}\right) \qquad (4)$$

Here E_δ is the local electric field (in the stacked sample zone), D is the molecular diffusion coefficient of the sample ions, l is the effective initial length of the region of sample to be stacked, and CI is the stacking ratio, in general CI = $C_{S,final}/C_{S,initial}$. CI scales as l/δ, where δ is the length scale of the stacked sample zone. This Pe_s can be used to compare relative importance of electromigration (which leads to sample stacking) and diffusion (which works against sample stacking). Equation 4 therefore suggests that large E_δ and large l lead to higher increases of sample concentration, two qualitative trends we observe in practice. E_δ is a function of applied field and the conductivities of the sample, LE, and TE zones. For example, for a given applied total potential, low TE concentration increases E_δ and should favor stacking.

l can be increased by injecting large, finite sample plugs. However, in practice, we find it is even more effective to increase the effective value of l by setting up a single-interface ITP process as shown in Figure 1a (inset). In this ITP configuration, the sample is initially uniformly dissolved into the TE and stacking is achieved in a zone between the TE and LE (see Figure 1b−d). In the current approach, the effective length of the sample plug is not limited by the channel geometry of the injection region as is the case for most on-chip ITP/CE work,[15,49,51] but by the duration of the ITP injection step where sample is allowed to flow into the channel (i.e., from the reservoir). In ITP, sample concentration first increases and then saturates at a "fully stacked" value. The width of the stacked sample region then increases indefinitely (albeit very slowly). For low initial sample concentration and high LE concentration (the case of most interest), we can expect the local field in the TE zone to be a strong function of the (growing) length of the TE zone and TE ion concentration. The relatively low conductivity TE zone is a high resistance in series with the rest of the channel. We hypothesize that TE concentration and TE zone length also strongly affects the stacked sample zone electric field, E_δ.

EXPERIMENTAL SECTION

Materials and Instrumentation. N-Hydroxyethylacrylamide (HEA) was purchased from Cambrex Bio Science (Walkersville, MD). V-50 initiator (2,2′-azobis(2-amidinopropane) dihydrochloride) was purchased from Wako Chemical USA (Richmond, VA). We synthesized polymers of HEA using free-radical polymerization in aqueous solution.[59] We used Alexa Fluor 488 and bodipy (Molecular Probes, Eugene, OR) as sample analytes. We used rhodamine B (Acros Organics, Morris Plains, NJ) as a neutral marker to quantify EOF. Sodium chloride, sodium hydroxide, and hydrochloric acid were obtained from Fisher Scientific (Pittsburgh, PA). TE and LE consist of 5 mM HEPES (pH 7.0; Sigma, St. Louis, MO) titrated with sodium hydroxide and 1 M NaCl (pH 5.3)
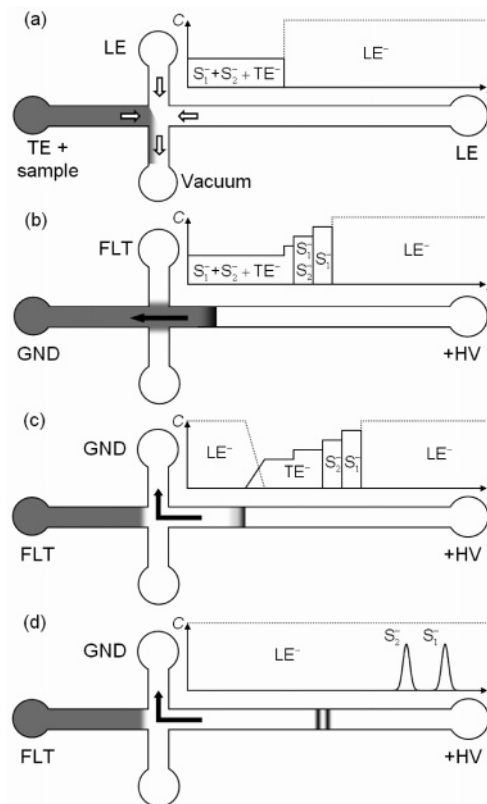
(58) Bharadwaj, R. Ph. D. Stanford University, Stanford, CA, 2005.
(59) Albarghouthi, M. N.; Stein, T. M.; Barron, A. E. *Electrophoresis* **2003**, *24*, 1166−1175.

Figure 1. Schematic of ITP/CE assay protocol. Configurations of co-ions are also shown at each step. (a) The north and the south reservoirs are filled with LE, and the west reservoir is filled with a mixture of TE and sample. TE/LE boundary is formed by applying vacuum at the south reservoir. White arrows show the direction of pressure-driven flows. (b) ITP stacking is initiated by applying high voltage and ground at the east and west reservoirs, respectively. The black arrow denotes the direction of electric field. Sample anions electromigrate toward the anode as EOF is suppressed. The early stage of ITP stacking results in a partial separation (i.e., moving boundary electrophoresis). (c) The field is switched toward the north reservoir to inject LE ions behind the sample and initiate CE. ITP stacking continues until LE ions overtake the TE and sample ions. (d) Separation of samples occurs further downstream where sample ions electromigrate in nearly homogeneous LE electrolyte (remnant of TE not shown).

dissolved in deionized water, respectively. HEPES ions, chloride ions, and sodium ions were the trailing ion, leading ion, and counterion, respectively. We added 0.1% w/v poly(N-hydroxyethylacrylamide) (PHEA) to all electrolytes to suppress EOF.[59] All electrolyte solutions were filtered prior to use with 0.2-μm pore syringe filters (Nalgene Labware, Rochester, NY).

We used a standard, cross-pattern glass microchip (Micralyne, Alberta, Canada) with channels 50 μm wide and 20 μm in depth. Images of the sample injection, stacking, and separation process were captured with an inverted epifluorescent microscope (IX70; Olympus, Hauppauge, NY) with 4× (NA of 0.16), 10× (NA of 0.4), and 20× (NA of 0.5) objectives (Olympus, Hauppauge, NY) and an XF100-3 filter cube (Omega Optical, Brattleboro, VT) with peak excitation and emission wavelength ranges of 450−500 and 500−575 nm, respectively. Images were recorded using a generation III, intensified CCD camera (IPentaMAX; Roper Scientific, Trenton, NJ) with a 12-bit intensity digitization resolution. A LabVIEW-controlled high-voltage power supply (Micralyne) was used to control electric field for ITP/CE process.

ITP/CE Protocol. We have developed a hybrid ITP/CE method for microchip-based CE devices. The injection method is depicted schematically in Figure 1. The four steps can be summarized as follows: (i) We perform a microchannel glass surface pretreatment where the entire microchannel is washed with 1 M HCl for 15 min. This is followed by flushing with 0.1% w/v PHEA solution for 15 min. (ii) Sample is loaded and the TE/LE interface formed. Here, a high-conductivity LE buffer is loaded into the separation channel reservoir and a side channel reservoir (designated as east and north in the figure, respectively). A mixture of sample and low-conductivity TE buffer is then loaded in the sample (west) reservoir. An interface TE/LE boundary is formed at the cross-intersection of microchip by applying vacuum for 10 s at the sample waste (south) reservoir. To avoid siphoning into the south reservoir after vacuum, we used a conical plastic pipet tip as a vacuum inlet (typical volume of 100 μL) to reduce local pressure at the south reservoir and yet maintain sufficient liquid in the well. (iii) The stacking step is next. Once the TE/LE boundary is established, an electric potential is applied at the east reservoir and the west reservoir is grounded, forming an east-to-west electric field. This electric field initiates electrophoretic migration of both sample and trailing ions into the separation channel and ITP stacking. (iv) Separation and detection is achieved. Here, the electric field is switched toward the north reservoir by floating the west reservoir and grounding the north reservoir. In this key step, the ITP mode is terminated by injecting leading electrolyte into the separation channel. Although the stacked sample zone is now well downstream of the intersection (typically 5−20 mm downstream), the leading ions overtake first trailing ions and then sample ions in the separation channel. This replacement of TE with LE effects an electrolyte exchange, terminating ITP stacking and initiating CE separation. Separated sample peaks are then detected downstream (using an epifluorescent microscope and a CCD camera). Our ITP/CE protocol is different from previous single-column or coupled-column ITP/CE protocols in that it avoids manual buffer exchange steps (e.g., as employed by Xu et al.[60]), so that the transition from ITP to CE mode therefore occurs abruptly and with minimum dispersions. Our ITP/CE protocol also achieves fast exchange of background electrolyte for CE mode by introducing leading electrolyte in the midst of trailing electrolyte/sample region (compared to capillary injections, which require injection of LE at the far-upstream inlet of the capillary). The protocol is also accomplished with a standard four-well chip and without feedback control of injections (e.g., in contrast to the five-well chip and feedback control used by Wainright et al.[51]).

Intensity Normalization. The concentration of sample ions can change 6 orders of magnitude during the ITP stacking process. Since the dynamic range of CCDs or PMTs is limited, simultaneous detection of both the initial and stacked sample intensities is difficult in a single experiment. The dilute sample signal can be below the LOD of the system, while that of a stacked sample may saturate the detector. To accommodate this, we applied a quantitative (and calibrated) imaging technique. The measured sample concentration, C_S, is

(60) Xu, Z. Q.; Nishine, T.; Arai, A.; Hirokawa, T. *Electrophoresis* **2004**, *25*, 3875−3881.

$$C_S = C_{flat}\frac{I_{raw} - I_{bg}}{I_{flat} - I_{bg}} \qquad (5)$$

where C_{flat} is the known concentration of highly concentrated sample analyte for the flatfield measurement and I_{raw}, I_{flat}, and I_{bg} are respectively the signal intensities of stacked sample, flat field, and background without sample (the latter with shutter open and illumination as normal). The flat-field image was obtained by imaging the microchannels filled with a homogeneous concentration of dye with a molar concentration $1 \times 10^3 - 1 \times 10^5$ times higher than (unstacked) initial sample concentration.

RESULTS AND DISCUSSION

To minimize dispersion due to EOF mismatch (see discussion of eq 3 above), we treated the microchannel walls with hydrophilic polymers. To validate this EOF suppression method, we measured electroosmotic mobility by injecting rhodamine B as a neutral dye. The electroosmotic mobilities of untreated and coated borosilicate microchannel were 5.9×10^{-8} m^2/V·s and 2.0×10^{-9} m^2/V·s, respectively; so that the PHEA coating reduces EOF to 3.4% of the untreated value (this small-magnitude, negative EOF mobility serves to slightly increase possible sample injection times prior to separation and detection).

We verified the dependence of signal intensity of the fluorophore on different background electrolytes and their pH values. We measured the signal intensity of fluorescent sample analytes ranging from low concentration (1 nM) to high concentration (10 μM), each using the following solvents: deionized water (pH 5.4, which is typical of deionized water exposed to the atmosphere), TE (5 mM HEPES buffer, pH 7.0), and LE (1 M NaCl, pH 5.3). The measured signal intensity of the Alexa Fluor dye was linearly proportional to the sample concentration in all cases (typical regression coefficients were $R^2 = 0.9993 - 0.9998$) and varied by less than 5.0% across solvents. The signal data can be interpreted as measurements of absolute sample concentration.

We tailored the voltage scheme of our ITP/CE method to our chip and detection system. Critical parameters in this customization include applied electric field strength (we limited this to values below which Joule heating was detectable from voltage versus current curves) and the duration of the stacking step (step iii of the ITP/CE protocol). Figure 2 shows a schematic of typical curves of maximum concentration versus separation channel location for the current ITP/CE process. Several traces of actual data are overlaid for reference. In the ITP mode, sample peak signal intensity first increases approximately linearly and eventually saturates. Upon initiation of the CE mode, sample concentration scales as the square root of time (and $x^{0.5}$) due to diffusion. For the overlaid experimental curves, the applied field and initial sample concentration were 110 V/cm and 100 nM and the duration of stacking step was varied between 5 and 10 s. As shown, the maximum achievable concentration can be limited by the effective injected sample length as determined by the duration of the ITP step.

We first summarize the variation of electric field, injection time, and detector location. In general, an overly long duration of sample injection (during ITP mode) results in a CE separation process further downstream (see Figure 2), while overly short sample injection durations terminate ITP mode before achieving the fully
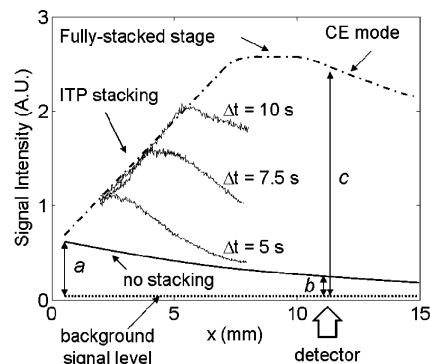
Figure 2. Schematic and various measurements of typical signal intensity changes in ITP/CE. Three specific signal intensities points are shown: The original, upstream sample intensity, a, the intensity of analyte detected at the downstream for "no stacking" conditions, b, and the intensity of the stacked analyte detected at the downstream, c. Two figures of merit are the ratios c/a and c/b, which are respectively the concentration increase, CI, and the signal increase, SI. Sample injection time was varied from 5 to 10 s. LE and TE were respectively 50 mM NaCl and 5 mM HEPES. The potential drop between the electrodes during stacking process was 1 kV (nominal electric field of 110 V/cm). We used 2× objective (NA of 0.08) with viewing area of 6.0 by 0.1 mm in the object plane.

stacked state (i.e., the plateau in signal in Figure 2). The former adversely affects resolution while the latter lowers signal-to-noise ratio (SNR). Long sample injection leads to lower resolution since sample analytes have less time to separate before reaching the detector. Long sample injection therefore requires longer separation channel lengths and run times. For our cases of interest, we obtained good stacking and separation results for a 40-s sample injection/ITP duration with a nominal electric field of 220 V/cm and a detection point 30 mm downstream.

We also performed an experimental parametric study to empirically optimize the ITP/CE process in our chip, demonstrate the strengths and weaknesses of the simple theory presented earlier, and provide validation data for future modeling efforts. We focused on the variation of three key parameters: the concentrations of LE, TE, and the initial sample concentration. These parametric studies were performed without the CE step (step iv of the ITP/CE protocol) with a fixed detector location (30 mm downstream from the injector region). We also confirmed that all cases reached a fully stacked state (i.e., a plateau) by verifying the transients of the stacking procedure using full-field imaging at low magnifications.

The effects of LE (NaCl) concentration, C_{LE}, TE (HEPES) concentration, C_{TE} and initial concentration of sample (Alexa Fluor), $C_{S,initial}$ on sample stacking are summarized in Figure 3. Fluorescent signals were detected with a viewing area 3.0 by 0.3 mm in the object plane at a point 30 mm downstream from intersection. All signals reached a fully stacked state within this distance from the intersection and during step iii of the ITP/CE protocol. The exposure time and frame rate were respectively 10 ms and 20 frames/s. All cross-sectional-area-averaged axial intensity profiles were normalized as per eq 5.

C_{LE} was first varied from 10 mM to 1M to study its effect on maximum stacked sample concentration, $C_{S,final}$, and CI (Figure 3a). The error bars in this and Figure 4 below reflect 95% confidence intervals as determined from three realizations of each condition. Here, TE was fixed at a nominal value of 5 mM HEPES.
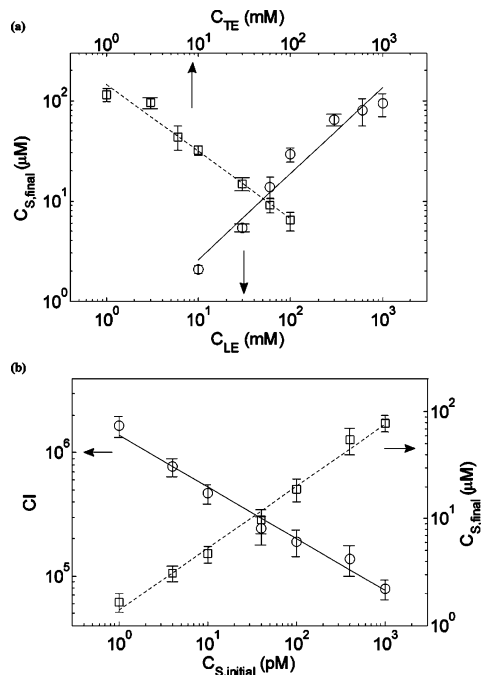

Figure 3. Parametric variations of initial concentration profile. The nominal applied field was 220 V/cm. CCD viewing area was centered 30 mm downstream of the channel intersection. (a) Maximum stacked sample concentration, $C_{S,final}$, versus LE concentration, C_{LE}, and TE concentration, C_{TE}. For variation of C_{LE}, sample analyte and TE were respectively 1 nM Alexa Fluor 488 and 5 mM HEPES. The regression coefficient, R^2, is 0.95. For variation of C_{TE}, sample analyte and LE were respectively 1 nM Alexa Fluor 488 and 1 M NaCl. $R^2 = 0.97$. (b) CI and $C_{S,final}$ versus initial sample concentration, $C_{S,initial}$. TE and LE were 5 mM HEPES and 1 M NaCl, respectively. The regression coefficients for CI and $C_{S,final}$ are respectively 0.97 and 0.98.

The TE solution contained 1 nM Alexa Fluor 488 as a sample analyte. The associated LE-to-TE conductivity ratios were between 13.9 and 1.21×10^3. The stacked sample concentration is nearly directly proportional to the concentration of LE ($R^2 = 0.95$ for a linear fit), as expected from the nondispersive 1D model. However, the simple model drastically underpredicts the proportionality constant; the measured stacked sample concentrations are 3500−7900-fold less than that predicted by eq 2, despite the fact that all cases reached fully stacked state (i.e., a plateau in the concentration versus distance relation).

Figure 3a also shows the effect of C_{TE} on ITP stacking where we varied C_{TE} from 1 to 100 mM. The LE was fixed at 1 M NaCl, and $C_{S,initial}$ was fixed at 1 nM. The associated LE-to-TE conductivity ratios were between 66.2 and 6.01×10^3. Recall that the nondispersive 1D model suggests that stacked sample concentration is not a function of $C_{S,initial}$ or C_{TE}. However, the measurements show that $C_{S,final}$ increased for lower C_{TE} (i.e., as conductivity ratio increases). We attribute this to the dependence of local field in the TE zone and stacked sample on TE concentration and the effects of dispersion. High LE-to-TE conductivity ratios (associated with low TE concentrations) increase the electric fields in the TE zone and the stacked sample zones. High electric field in the TE zone leads to fast stacking dynamics as there is a high electrophoretic flux of sample from the TE zone to the stacked sample zone. We hypothesize that high E_δ leads to high electric Peclet numbers (eq 4) and therefore high $C_{S,final}$, as the stacking process is less susceptible to dispersion.

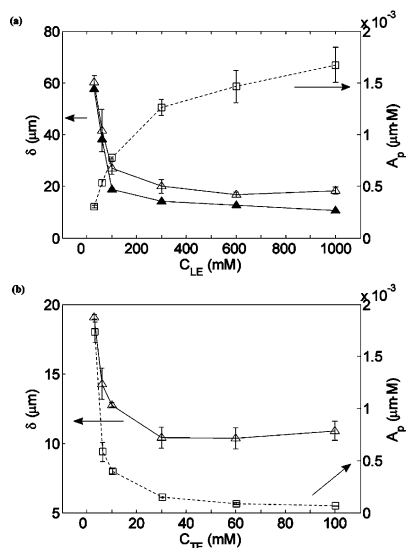**Figure 4.** Plots of peak width measurement from image data, δ_i, peak width estimate from a one-dimensional analysis, δ_{est}, and area, A_p, of stacked sample peaks. We characterized δ_i and A_p as respectively twice the standard deviation of a fitted Gaussian and the product of peak width and peak height. Sample was 1 nM Alexa Fluor 488. (a) Peak width and A_p as a function of C_{LE} with TE fixed at 5 mM HEPES. Open triangles show peak width measurements from image data, δ_i. Closed triangles show an estimate of sample width, δ_{est}, based on measured peak concentration and the sample flux in the TE region. (b) δ_i and A_p as a function of C_{TE} with LE fixed at 1 M NaCl. A 4× objective (NA of 0.16) was used for these measurements.

Next, we varied $C_{S,initial}$ from 1 pM to 1 nM as shown in Figure 3b. The LE and TE were respectively fixed at 1 M NaCl and 5 mM HEPES. The LE-to-TE conductivity ratio was kept constant at 1.27×10^3 (113 mS/cm for LE and 89.0 μS/cm for TE) for all cases in an effort to decouple the results from the effect discussed above (i.e., the dependence of the TE zone electric field and E_δ on LE-to-TE). Note that the effect of sample ions on electrical conductivity of the TE/sample mixture was negligible as $C_{S,initial} \ll C_{TE}$. The data show CI increases as $C_{S,initial}$ decreases. This result is consistent with the 1D nondispersive model. However, note that the dependence of CI on $C_{S,initial}$ is weaker than the inversely proportional dependence predicted by the simple model (CI changes just under 2 orders of magnitude while $C_{S,initial}$ changes 3 orders of magnitude). This discrepancy is also apparent in the measurements of the maximum concentration, $C_{S,final}$. The model predicts that $C_{S,final}$ should not be a function of $C_{S,initial}$. However, the experimental data show that $C_{S,final}$ is a linear function of (although not directly proportional to) $C_{S,initial}$. This result is not attributable to changes in local field in the TE zone. Note that all measurements shown in Figure 3 were obtained in the fully stacked zone (e.g., flat region of the top curve of Figure 2). Clearly, more comprehensive models are required to capture the complexity of the current ITP stacking dynamics.

The width of sample analyte peaks also strongly depends on LE and TE concentration, and such data are important for validation of models of ITP that include both diffusion and advective dispersion effects. Figure 4 shows plots of the measured characteristic width, δ_i, and the area of sample peaks, A_p, for various LE and TE concentrations as determined from the image data. We characterized peak width as twice the standard deviation

of a Gaussian fit to the peak. Peak area was estimated by multiplying peak width by peak heights and is a measure of the amount of sample in the peak. In these data, we varied C_{LE} from 30 mM to 1 M, while the TE and sample were fixed at 5 mM HEPES and 1 nM Alexa Fluor 488, respectively. δ_i decreased as C_{LE} increased. This is consistent with the results of Figure 3 (and with the simple model) since higher C_{LE} allows larger stacking ratio and so sample analytes can be focused more narrowly. To show consistency, Figure 4a also shows stacked sample peak widths as estimated from a simple control volume analysis and the CI measurements. This estimated sample peak width, δ_{est}, uses a simple resistor model for the TE and LE regions to determine the electric field and electrophoretic sample flux in the TE region. This sample flux is then assumed to accumulate directly into a Gaussian peak with a peak value of the measured maximum concentration. The peak width estimate is then simply $\delta_{est} \simeq (2/\pi)^{1/2}\nu_S\bar{E}\Delta t/$CI, where $\bar{E}$ is the time average electric field in the TE region (which varied from 2.0 to 2.8 kV/cm), Δt is stacking duration (50–110 s), and ν_S is sample mobility (4.2×10^{-8} m^2/V·s). As shown in Figure 4a, this simple scaling actually captures the imaged peak width trends quite well. The δ_{est} model underpredicts sample peaks at high C_{LE}, and this is probably due to the limitations of the simple model. For example, the actual concentration distribution is not 1D as assumed by the δ_{est} estimate. A slight deformation of the peak region (e.g., along the channel depth) would show up in the image data as an apparent increase in peak width.

Figure 4a also shows that A_p also increased as C_{LE} increased. For the ITP processes used here, the sample width is expected to increase indefinitely during the ITP step as more sample ions are transferred from the zone of TE/sample mixture to the sample zone. We hypothesize that, for higher C_{LE} values, a higher fraction of the total voltage drop is taken along the length of the TE region, increasing the flux of sample into the sample zone. This causes the peak to have lower migration velocity and higher stacking ratio. For increased C_{LE}, therefore, peak widths have a longer time to grow before being detected at the (fixed) detection point 30 mm downstream. This hypothesis is supported by an analysis of the transient data and by (full-field CCD image) measurements performed at a location just 1.5 mm downstream of the injector region. The latter observations show that lower C_{TE} and higher C_{LE} each result in larger slopes in curves of maximum (stacked zone) concentration versus separation channel distance, x. These data also suggest that lower C_{TE} cases reach the fully stacked state at relatively short distances, while higher C_{LE} cases reach the fully stacked state at long distances.

Next, we varied C_{TE} from 3 to 100 mM, while LE and sample were fixed at 1 M NaCl and 1 nM Alexa Fluor 488, respectively. As shown in Figure 4b, δ_i decreased as C_{TE} increased. Higher C_{TE} (with fixed C_{LE}) implies higher conductivity in the TE/sample zone. This lowers the TE/sample zone electric field and decreases the rate of stacking, increasing the time (and distance) to reach the fully stacked state. For the fully stacked states shown in Figure 4, therefore, the widths of the sample zone are narrower for high C_{TE} as the sample peak has had less time to accumulate width. This effect and the lower final concentration value (see Figure 3b) result in lower peak areas for higher C_{TE}.
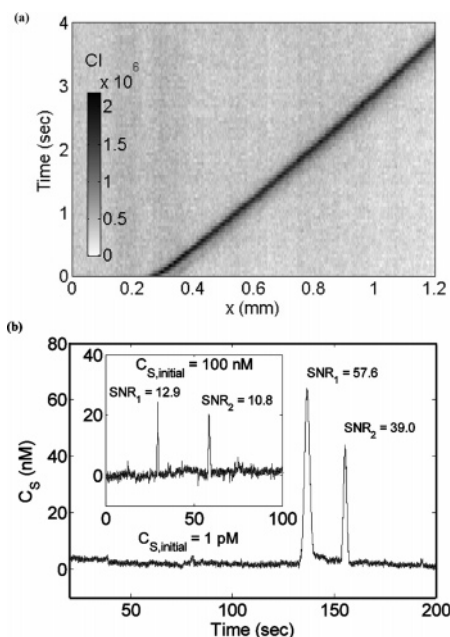
Figure 5. Demonstration of ITP and ITP/CE protocol processes. (a) Detection of Alexa Fluor 488 with an initial concentration of 100 fM resulted in greater than millionfold concentration increase. LE and TE were respectively 1 M NaCl and 5 mM HEPES. We used a 10× objective (NA of 0.4). (b) Comparison of ITP/CE and CE separations of Alexa Fluor 488 (first peak) and bodipy (second peak). The position of the detector is 30 mm downstream of injector region. A 20× objective (NA of 0.5) was used. Inset electropherogram shows separation (with no stacking) of 100 nM initial concentrations of Alexa Fluor 488 and bodipy. 5 mM HEPES used as a background electrolyte and applied electric field was 280 V/cm. For ITP/CE mode (main plot), initial concentrations of Alexa Fluor 488 and bodipy were both 1 pM in 5 mM HEPES (i.e., diluted by a factor of 1×10^5). Here, LE was 1 M NaCl and nominal applied field was 220 V/cm. The concentration increase, CI, and signal increase, SI, for Alexa Fluor 488 (first peak) are 6.4×10^4 and 4.5×10^5, respectively.

We also demonstrated the detection of a trace analyte using ITP stacking alone. Figure 5a shows a spatiotemporal intensity plot of CI versus separation channel location and time from which sample peak reaches the detection window, for an initial sample concentration of 100 fM Alexa Fluor 488 dye. The LE was 1 M NaCl, and the TE was 5 mM HEPES buffer. We used a 10× objective (NA of 0.4) with viewing dimensions of 1.2 by 0.1 mm in the object plane. A brief (~2 min) sample stacking step enables the detection of 100 fM analyte concentration with SNR = 11. Measured concentration distributions yield a maximum measured concentration increase, CI, of ~2×10^6-fold. This concentration increase is achieved within 120 s and 30 mm downstream of the injection point.[61] To our knowledge, this is the highest sample preconcentration for either capillary or on-chip electrophoresis systems.

Last, we demonstrated the effectiveness of the ITP/CE protocol with separations of Alexa Fluor 488 and bodipy. Figure 5b shows the separations of sample analytes detected 30 mm downstream

of the intersection without (inset) and with ITP stacking. The electropherograms are determined by spatially integrating full-field CCD imaging data over a 60 by 60 μm region centered on the channel centerline to simulate the detection of a pointwise photodetector. The exposure time and CCD frame rate were 10 ms and 50 frames/s, respectively. The inset of Figure 5b shows the separation without ITP with initial (relatively high) concentrations of 100 nM and a uniform background electrolyte consisting of 5 mM HEPES buffer (pH 7.0). Signal intensity was normalized using the flat-field image signal of 100 nM Alexa Fluor 488. The applied field was 280 V/cm. The SNRs of Alexa Fluor 488 (first peak) and bodipy (second peak) are 12.9 and 10.8, respectively, and the peak resolution is 29.4. We define SNR as the ratio of peak intensity to twice the standard deviation of background noise and resolution as the distance between two peaks divided by the full width half-maximum of the wider peak.[62] We then performed separation of this sample mixture diluted by a factor of 1×10^5 (1 pM solutions each of Alexa Fluor 488 and bodipy) and applied the current ITP/CE method. The result is shown in Figure 5b. The injection/ITP time was 40 s, and we used a nominal applied field of 220 V/cm. The resolution of these peaks is 6.1, and the SNRs are respectively 57.6 and 39.0 for Alexa Fluor 488 and bodipy. The ITP phase of the experiment shown in Figure 5b achieved a concentration increase of ~0.5 million-fold immediately prior to initiation of the CZE mode. This experiment achieves a concentration increase of 6.4×10^4 relative to the initial sample concentration (1 pM) and a signal increase of 4.5×10^5-fold relative to the unstacked case.

SUMMARY

ITP provides self-sharpening peaks and can be integrated with CE separation. An 1D nondispersive model and scaling of dispersion analysis yield important insight into key ITP stacking parameters and suggest strategies for optimizing ITP in practice. These strategies include using high LE concentration and low initial sample concentration to maximize achievable concentration increase, suppression of EOF to minimize dispersions, and implementation of a single-column ITP configuration (where initially there is a single interface between the LE and the TE/sample mixture) to inject a large effective sample width. We have implemented these strategies in the design of an ITP/CE method that combines a simple and robust single-column ITP stacking step with a subsequent CE step. We first injected a sample/TE mixture to initiate ITP stacking and then injected LE at the channel intersection. The latter LE ion stream overspeeds TE ions behind the stacked sample zone, terminates ITP, and initiates CE separation.

We performed an experimental parametric study focused on the variation of LE, TE, and initial sample concentration. Consistent with the 1D nondispersive model, we found that stacked sample concentration is proportional to the LE concentration, and the concentration increase, CI, (conveniently) increases as the initial sample concentration decreases. We also found that the stacked sample concentration is a strong function of the TE concentration and the initial sample concentration. For our configuration, low-conductivity TE zones result in higher TE zone

(61) Direct measurement of peak width for this high CI case is difficult with fluorescence imaging. The smallest length scales we can resolve are ~3 μm (the pixel dimension projected into the object plane is 2.4 μm and the channel depth and depth of field are respectively 20 and 3 μm). The simple 1D model estimate described earlier suggests a value of $\delta_{est} \simeq 1$ μm for this CI = 2×10^6 experiment.

(62) Bharadwaj, R.; Santiago, J. G.; Mohammadi, B. *Electrophoresis* **2002**, *23*, 2729−2744.

electric fields and therefore faster rates of stacking. High TE zone fields are probably also correlated with high stacked zone fields, E_δ. We hypothesize that this, combined with the large effective injection length of the single-interface ITP configuration, results in large sample electric Peclet numbers and efficient stacking that is less susceptible to dispersion. Results suggest that comprehensive multispecies models with coupled fluid flow (including perhaps effects of nonuniform and dynamic zeta potentials), current conservation, and convective-diffusion-electromigration conservation are needed to fully describe ITP. Inclusion of reaction buffer kinetics may also be important.

Detection of trace of Alexa Fluor 488 was demonstrated with a maximum stacking ratio of 2×10^6-fold in 2 min and an LOD of 100 fM (SNR = 11). We also analyzed the separation of Alexa Fluor 488 and bodipy using our ITP/CE protocol and demonstrated a CI of 6.4×10^4-fold and signal increase of 4.5×10^5-fold (in a 160 s combined ITP and CE process). Future work will include the formulation and validation of more comprehensive models for the ITP protocol proposed here and further applications of the ITP/CE protocol.